Sub-Cycle Dynamic Phasors With Adjustable Transient Response

Afsaneh Ghanavati, *Member, IEEE*, Hanoch Lev-Ari, *Fellow, IEEE*, and Aleksandar M. Stanković, *Fellow, IEEE*

Abstract-We extend in several directions the study of our fast sparse alternative to the standard (FFT-based) evaluation of dynamic phasors. We present analysis for an arbitrary shift between the waveform samples used to construct sub-cycle dynamic phasors. Next, we show that the transient response of sub-cycle dynamic power metrics can be improved by using a small number of waveform samples and adjusting the uniform inter-sample shift. Our real-life examples demonstrate that reduction of the inter-sample shift can be quite effective in the presence of fast transients (wide-band in frequency). We use a synthetic example to demonstrate that a metric obtained from a sub-cycle scheme provides surprisingly accurate information about the duration and onset-time of a transient. We also identify a range of shift values for which the steady-state error remains near-optimal, and we derive conditions for a superior performance for slow transients. Finally, our results suggest that in practical real-time implementations it may be advantageous to calculate at least two sets of phasors to cover both slow and fast transients: the computational cost of such a scheme is still significantly lower than that of a standard full-cycle calculation.

Index Terms—Structured sparse Fourier transform, sub-cycle, dynamic phasors, dynamic power metrics, fast power system transients, slow power system transients.

I. INTRODUCTION

PHASOR Measurement Units (PMUs) are an example of the new generation of high-bandwidth sensor that holds the promise to enable operation of future hybrid energy grids combining inverter-connected and conventional electromechanical sources. One novel aspect that such sensors bring into AC grids is the generation of large, continuous data streams. For

Manuscript received June 6, 2019; revised September 21, 2019; accepted November 2, 2019. Date of publication November 28, 2019; date of current version July 23, 2020. This work was supported in part by ONR under Grants N00014-10-1-0538 and N00014-16-1-3028, in part by the National Science Foundation under Grant ECCS-1710944, in part by the NSF/DOE Engineering Research Center Program under NSF Award EEC-1041877, and in part by the CURENT Industry Partnership Program. Paper no. TPWRD-00619-2019. (Corresponding author: Aleksandar M. Stankovic.)

A. Ghanavati is with the Department of Electrical and Computer Engineering, Wentworth Institute of Technology, Boston, MA 02115 USA (e-mail: ghanavatia@wit.edu).

H. Lev-Ari is with the Department of Electrical and Computer Engineering, Northeastern University, Boston, MA 02115 USA (e-mail: levari@ece.neu.edu).

A. M. Stanković is with the Department of Electrical and Computer Engineering, Tufts University, Medford, MA 02155 USA (e-mail: astankov@ece.tufts.edu).

Color versions of one or more of the figures in this article are available online at http://ieeexplore.ieee.org.

Digital Object Identifier 10.1109/TPWRD.2019.2956637

example, a typical PMU generates a phasor once every cycle of the fundamental, yielding 100 Gb a year [1] of data. There are likely more than 10,000 PMUs installed today [2] producing more that 1,000 Tb every year. For certain detailed analyses of transients, it would be desirable to record the input data into PMUs, which would result in another increase of more than two orders of magnitude, as the sampling frequency is typically of the order of 10 kHz [3].

Pre-processing and possible compression of the input- and output-data sets for PMUs is thus a growing research endeavor. The goal is to retain advantages of fast sampling, such as precise and timely detection of events, while reducing the data set by pruning away the less-relevant content. A general real-time data compression is applied in [4] to wide-area measurement system, while a tailored compressed sensing algorithm is applied to PMU data in [5]. The principal component analysis (PCA) is tested on PMU data in [6], while data streaming aspects are explored and quantified in [2].

A pertinent body of theoretical work is known in the literature as sparse Fourier Transform [7]. When analyzing large data sets, the sparse Fourier transform (SFT) computes a compressed Fourier transform from only a small subset of the input data. It turns out that our approach introduced in [8] can be described as a highly structured SFT. Our method leverages the strong prior information about the nominal fundamental frequency ω_0 , and the likely harmonic content of energy system waveforms (e.g., odd waveforms, near absence of triplen harmonics), and uses it to devise algorithms that are simpler and computationally cheaper.

The key idea here is that using the (very inexpensive) subcycle scheme as a front end processor that facilitates reduced storage. In other words, instead of storing many full-cycle phasors, we propose to store a few sub-cycle phasors or, alternatively, a few sub-cycle dynamic power quality metrics (DPQMs). Our algorithms achieve a major reduction of computational cost, as compared with both SFT (which is not designed to be dynamic), and full-cycle (which uses a large set –128 to 256 samples per cycle). In contrast, we only use a few samples at each time instant to evaluate dynamic sub-cycle phasors. In addition, the dynamic phasors and sub-cycle DPQMs can prove useful for detecting, classifying and monitoring faults.

While this paper is conceptually in the same vein as [8], it extends it in several key ways: (1) We present analysis for an arbitrary shift Δ between the M waveform samples used to construct sub-cycle dynamic phasors. The scheme presented in [8] relied on the special choice $\Delta = \frac{T}{2M}$ (where $T = \frac{2\pi}{\omega_0}$),

0885-8977 © 2019 IEEE. Personal use is permitted, but republication/redistribution requires IEEE permission. See https://www.ieee.org/publications/rights/index.html for more information.

which ensures low steady-state error, and induces a Parseval relation between waveform samples and sub-cycle dynamic phasors. (2) We show in this paper that the transient response of sub-cycle dynamic power metrics can be improved by reducing the value of the normalized shift $\xi \stackrel{\triangle}{=} \Delta/T$ towards $\frac{1}{4M}$, and using a small number of waveform samples. (3) Our real-life examples demonstrate that reduction of the normalized shift ξ can be quite effective in the presence of short transients (fast, wide-band in frequency): the N-metric (derived in Section VI from power flows, i.e., nonlinear in terms of voltage and current phasors) obtained from a 4-sample sub-cycle scheme with $\xi = \frac{1}{16}$ provides accurate information about the duration and onset-time of a transient. (4) We identify a range of ξ values for which steady-state error remains near-optimal, and (5) We show that setting M=8 and $\xi=\frac{1}{2M}$ results in excellent performance for slow transients. Taken together, our results suggest that in practical real-time implementations it may be advantageous to calculate at least two sets of phasors to cover the possibility of both slow and fast transients. Given the low cost of each calculation, the overall computational effort is still significantly below that of full-cycle calculations, while providing improved metrics for various classes of transients.

The rest of the paper is organized as follows: in Section II we introduce sub-cycle dynamic phasors for arbitrarily-shifted waveform samples; in Section III we analyze the uniform-shift sample pattern, and in Section IV we provide conditions for orthogonality of the waveform-to-phasor map. In Section V we present some relevant dynamic power quality metrics, and in Section VI we use real-life transient examples to illustrate the tradeoff between accuracy and agility provided by adjusting the inter-sample shift Δ .

II. SUB-CYCLE DYNAMIC PHASORS

In general, we consider a set of M arbitrarily-spaced polyphase (i.e., $1 \times m$ vector) samples, viz.,

$$\{x(t); x(t-\Delta_1); \dots; x(t-\Delta_{M-1})\}$$

where $\Delta_1 < \Delta_2 < \ldots < \Delta_{M-1}$. These include the most recent waveform sample x(t), as well as several previous (stored) samples, located at the time instants $t - \Delta_1$, $t - \Delta_2$, etc. We use these samples to generate a set of L polyphase phasors with harmonic indices k_1, k_2, \dots, k_L . As in [8], we propose to use the sample matching constraint $x(t - \Delta_i) =$ $\sqrt{2} \sum_{\ell=1}^{L} \Re \left\{ \widehat{X}_{k_{\ell}}(t) e^{jk_{\ell}\omega_0(t-\Delta_i)} \right\}$, namely,

$$\begin{pmatrix} x(t) \\ x(t-\Delta_1) \\ x(t-\Delta_2) \\ \vdots \\ x(t-\Delta_{M-1}) \end{pmatrix} = \sqrt{\frac{M}{2}} \, \mathcal{W}_M \begin{pmatrix} \widehat{X}_{k_1}(t) \, e^{jk_1\omega_0 t} \\ \vdots \\ \widehat{X}_{k_L}(t) \, e^{jk_L\omega_0 t} \\ \widehat{X}_{k_1}^*(t) \, e^{-jk_L\omega_0 t} \\ \vdots \\ \widehat{X}_{k_L}^*(t) \, e^{-jk_L\omega_0 t} \end{pmatrix}$$

$$(1) \begin{pmatrix} H_{k_1}(s) \\ H_{k_2}(s) \\ \vdots \\ H_{k_L}(s) \end{pmatrix} = \frac{1}{\sqrt{L}} \begin{bmatrix} I_L & 0_L \end{bmatrix} \, \mathcal{W}_M^{-1} \begin{pmatrix} 1 \\ e^{-s \, \Delta_1} \\ e^{-s \, \Delta_2} \\ \vdots \\ e^{-s \, \Delta_{M-1}} \end{pmatrix}$$
In other words, for every $h \in S$, the filter H (s) map

as an implicit characterization of the polyphase dynamic subcycle phasors $\{X_{k_1}(t), X_{k_2}(t), \dots X_{k_L}(t)\}$. Here \mathcal{W}_M is

a constant $M \times 2$ L matrix, viz.,

$$\mathcal{W}_M \stackrel{\triangle}{=} \begin{bmatrix} \psi_{k_1} & \psi_{k_2} & \dots & \psi_{k_L} | \psi_{k_1}^* & \psi_{k_2}^* & \dots & \psi_{k_L}^* \end{bmatrix}$$
(2a)

with columns given by

$$\psi_k = \frac{1}{\sqrt{M}} \left[1 \ e^{-jk\omega_0 \Delta_1} \ e^{-jk\omega_0 \Delta_2} \ \dots \ e^{-jk\omega_0 \Delta_{M-1}} \right]^\top$$
(2b)

We use the superscript \top to denote transposition, while * denotes conjugation without transposition. This formulation relies on two sets of design parameters: the set of waveform time-shifts $\Delta \stackrel{\triangle}{=} \{\Delta_1, \Delta_2, \dots, \Delta_{M-1}\}$ and the set of harmonic indices $\mathcal{S} \stackrel{\triangle}{=} \{k_1, k_2, \dots, k_L\}$. Together, these parameter sets determine the properties of the sub-cycle dynamic phasors $\widehat{X}_k(t)$ and of the associated power metrics.

The set of equations (1) has a unique solution for the phasors $\{X_k ; k \in \mathcal{S}\}$ only when $M \geq 2 L$, and \mathcal{W}_M has full column rank. However, since transient performance always improves when M is decreased (as we demonstrate in Section VI) we propose to use in the sequel M=2 L. This choice also reduces implementation complexity (i.e., minimal number of waveform samples is used for a given L). Assuming that Δ and S have been chosen to make the square matrix \mathcal{W}_M non-singular, we obtain the explicit expression

$$\begin{pmatrix} \widehat{X}_{k_1}(t) e^{jk_1\omega_0 t} \\ \widehat{X}_{k_2}(t) e^{jk_2\omega_0 t} \\ \vdots \\ \widehat{X}_{k_L}(t) e^{jk_L\omega_0 t} \end{pmatrix}$$

$$= \frac{1}{\sqrt{L}} \begin{bmatrix} I_L & 0_L \end{bmatrix} \mathcal{W}_M^{-1} \begin{pmatrix} x(t) \\ x(t - \Delta_1) \\ x(t - \Delta_2) \\ \vdots \\ \vdots \\ x(t - \Delta_{M-1}) \end{pmatrix}$$
(3a)

This waveform-to-phasor map is, in fact, a linear-time-invariant system, with a single (polyphase) input x(t) and L (polyphase) outputs. Notice that each phase of the row vector x(t) is mapped into its own phasor (i.e. there is no coupling between phases), and the corresponding set of filters is

$$\begin{pmatrix} H_{k_1}(s) \\ H_{k_2}(s) \\ \vdots \\ \vdots \\ H_{k_L}(s) \end{pmatrix} = \frac{1}{\sqrt{L}} \begin{bmatrix} I_L & 0_L \end{bmatrix} \mathcal{W}_M^{-1} \begin{pmatrix} 1 \\ e^{-s \Delta_1} \\ e^{-s \Delta_2} \\ \vdots \\ e^{-s \Delta_{M-1}} \end{pmatrix}$$
(3b)

In other words, for every $k \in \mathcal{S}$, the filter $H_k(s)$ maps x(t)into $\widehat{X}_k(t) e^{jk\omega_0 t}$ (see Fig. 1). This property of $H_k(s)$ is a consequence of the harmonics-blocking property.

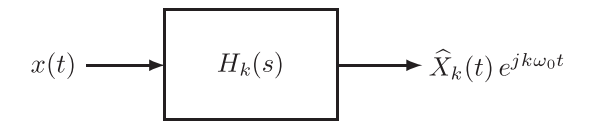


Fig. 1. Filtering interpretation of the waveform-to-phasor map (3a).

Theorem 2.1 (Harmonics-blocking property): Consider the transfer function $H_k(s)$ defined by (3b), for some $k \in \mathcal{S}$. The corresponding frequency response $H_k(j\omega)$ satisfies the constraints, for every $\ell \in \mathcal{S}$.

$$H_k(j\ell\omega_0) = \begin{cases} 0 & \ell \neq k \\ \sqrt{2} & \ell = k \end{cases}$$
 (4a)

$$H_k(-j\ell\omega_0) = 0 \tag{4b}$$

Proof: see Appendix.

In summary, for every $k \in \mathcal{S}$, the filter $H_k(s)$ passes the harmonic k, blocks the harmonic -k, and blocks all $\pm \ell$ harmonics for every $\ell \in \mathcal{S}$, $\ell \neq k$.

Consequently, when $\mathcal S$ matches the harmonic content of a periodic x(t), namely, $x(t) = \sum_{\ell \in \mathcal S} \sqrt{2} \, \Re\{X_\ell \, e^{j\omega_0 t}\}$, the resulting sub-cycle phasors match perfectly with the true phasors contained in x(t), i.e., they satisfy $\widehat X_k(t) = X_k$. However, if the input waveform x(t) contains harmonics that do not belong to $\mathcal S$, the filter will pass each such harmonic, say $r \notin \mathcal S$, with a gain of $H_k(jr\,\omega_0)$. The resulting sub-cycle phasor will be given by the (passband) expression

$$\widehat{X}_{k}(t) e^{jk\omega_{0}t} = X_{k} e^{jk\omega_{0}t} \frac{\sqrt{2}}{2}$$

$$+ \sum_{r \notin \mathcal{S}} \left[H_{k}(jr\omega_{0}) X_{r} e^{jr\omega_{0}t} + H_{k}(-jr\omega_{0}) X_{r}^{*} e^{-jr\omega_{0}t} \right]$$
(5)

Clearly, the average value of $\widehat{X}_k(t)$ is precisely X_k , while its instantaneous value fluctuates around this average. Thus, increasing the size of the harmonic index set \mathcal{S} , which reduces the number of spurious harmonics, results in lowering the level of $\widehat{X}_k(t)$ fluctuation, at the expense of an increased implementation cost. This steady-state fluctuation of $\widehat{X}_k(t)$, and its effect on dynamic power metrics, are discussed in further detail in Section III.

III. UNIFORM-SHIFT SAMPLE PATTERN

The complexity and implementation cost of the general expression (3a) can be significantly reduced by using uniformly-shifted waveform samples, namely,

$$\Delta_i = i \, \Delta, \quad i = 0, 1, 2, \dots, M - 1$$
 (6)

with the inter-sample shift Δ used as a design parameter. Our interest in improving the transient characteristics of the subcycle phasors $\widehat{X}_k(t)$ implies a preference for small values of Δ : we will be primarily interested in the range $0 < \Delta \leq \frac{T}{2M}$, where $T = \frac{2\pi}{\omega_0}$, as defined in Section I. The uniform-shift pattern (6) makes \mathcal{W}_M into a Vandermonde matrix: its columns are

given by

$$\psi_k = \frac{1}{\sqrt{M}} \begin{bmatrix} 1 & \alpha_k & \alpha_k^2 & \dots & \alpha_k^{M-1} \end{bmatrix}^\top \tag{7}$$

where $\alpha_k \stackrel{\triangle}{=} e^{-jk2\pi\xi}$, with $\xi \stackrel{\triangle}{=} \frac{\Delta}{T} > 0$, a normalized intersample shift. This rectangular Vandermonde matrix is nonsingular if, and only if, its columns are all distinct. This constraint limits the selection of harmonic indices for $\mathcal S$ because:

- When ξ is rational (i.e., $\xi = \frac{m}{D}$ for some integers m and D), which is always the case in a sampled-data implementation, the expression (7) for ψ_k is periodic in k with period D. Thus the only distinct choices for the parameters α_k are obtained when $0 \le k \le D 1$.
- In addition, $\psi_k^* = \psi_{D-k}$ for every $0 \le k \le D-1$. To avoid duplicate columns in \mathcal{W}_M we must impose the constraint $k + \ell \ne D$ for every $k \in \mathcal{S}$ and every $\ell \in \mathcal{S}$ (including the case $k = \ell$).

Choices of $\{S, \xi\}$ that results in a non-singular W_M will be called *feasible*.

Since typical power system (voltage and current) waveforms contain primarily odd harmonics, it makes sense to choose \mathcal{S} as a subset (of size L) of the odd harmonic indices in the range $[0\ D-1]$, subject to the constraint that for every $k\in\mathcal{S}$, the complementary value D-k cannot be included in \mathcal{S} . In addition, the index set \mathcal{S} should always include the fundamental harmonic. There is a limited number of such choices, which we call *primary*. For instance consider the case M=4, with the special choice $\xi=\frac{1}{2M}$, so that D=2 M=8, and the collection of possible (odd) index choices is $\{1,3,5,7\}$. The set $\mathcal{S}=\{k_1,k_2\}$ is constructed by selecting two of these, subject to the constraint $k_1+k_2\neq 8$. Thus the only feasible primary choices for \mathcal{S} are $\{1,3\}$ or $\{1,5\}$.

The transfer function $H_k(s)$ associated with a uniform-shift pattern is a polynomial in $e^{-s\Delta}$ (recall (3b)), with roots specified by Theorem 2.1. This observation leads to compact explicit expressions for both $H_k(s)$ and $H_k(j\omega)$.

Theorem 3.1 (Polynomial property): When $\Delta_i = i\Delta$, the transfer function $H_k(s)$ is a polynomial of degree M-1 in $e^{-s\Delta}$ (for every $k \in \mathcal{S}$), viz.,

$$H_k(s) = \mathcal{C}_k \left(1 - e^{-jk\omega_0 \Delta} e^{-s\Delta} \right)$$

$$\times \prod_{\ell \in \mathcal{S}, \ \ell \neq k} \left(1 - e^{j\ell\omega_0 \Delta} e^{-s\Delta} \right) \left(1 - e^{-j\ell\omega_0 \Delta} e^{-s\Delta} \right)$$
(8a)

where the value of the scaling coefficient C_k can be determined from the constraint $H_k(jk\omega_0) = \sqrt{2}$. The corresponding frequency response is

$$H_{k}(j\omega) = \sqrt{2} e^{-j(\frac{\omega}{\omega_{0}} - k)(M - 1)\pi\xi} \times \frac{\sin(\frac{\omega}{\omega_{0}} + k)\pi\xi}{\sin(2k\pi\xi)} \prod_{\ell \in \mathcal{S}, \ \ell \neq k} \frac{\sin(\frac{\omega}{\omega_{0}} + \ell)\pi\xi}{\sin(\ell + k)\pi\xi} \cdot \frac{\sin(\frac{\omega}{\omega_{0}} - \ell)\pi\xi}{\sin(\ell - k)\pi\xi}$$
(8b)

where $\xi \stackrel{\triangle}{=} \frac{\Delta}{T}$ is the normalized delay parameter.

Proof: see Appendix.

Corollary: The group-delay associated with $H_k(j\omega)$ is constant and proportional to ξ (equivalently to Δ), viz.,

group-delay
$$\stackrel{\triangle}{=} -\frac{d}{d\omega} \arg H_k(j\omega) = \xi\left(\frac{M-1}{2}\right)T$$
 (9)

It is evident from (5) that the sub-cycle phasor $\widehat{X}_k(t)$ fluctuates in steady-state around its true value X_k . The mean-square level of this fluctuation is given by

$$\begin{split} &\frac{1}{T} \int_0^T \left| |\widehat{X}_k(t) - X_k| \right|^2 dt \\ &= \sum_{r \notin S} \frac{\left[|H_k(jr\omega_0)|^2 + |H_k(-jr\omega_0|^2] \right]}{2} \left| |X_r|^2 \end{aligned} \tag{10a}$$

where (recall (8b))

$$|H_k(jr\omega_0)| = \sqrt{2} \frac{\sin(r+k)\pi\xi}{\sin(2\pi k \,\xi)} \prod_{\ell \in \mathcal{S}, \, \ell \neq k} \frac{\sin(r+\ell)\pi\xi}{\sin(\ell+k)\pi\xi} \frac{\sin(r-\ell)\pi\xi}{\sin(\ell-k)\pi\xi}$$
(10b)

Thus, the level of fluctuation depends on the value of ξ , the selection of the harmonic index set \mathcal{S} , and the magnitudes $|X_r|$ of the spurious harmonics of x(t), i.e., those harmonics that are excluded from \mathcal{S} . Since the group-delay of $H_k(j\omega)$ is $\Delta\left(\frac{M-1}{2}\right)=\xi\frac{(M-1)T}{2}$, the expression (10b) suggests that ξ can be used as a design parameter that controls a tradeoff between transient response and steady-state error (= level of fluctuation): as ξ increases from zero, the group-delay of $H_k(j\omega)$ increases (linearly in ξ), while the rms fluctuation tends to decrease (see, e.g., Fig. 2).

IV. ORTHOGONAL WAVEFORM-TO-PHASOR MAP

A particularly simple waveform-to-phasor map is obtained when the square matrix \mathcal{W}_M is orthogonal, namely $\mathcal{W}_M^{-1} = \mathcal{W}_M^H$. Under orthogonality, the expression (3b) reduces to

$$H_k(s) = \frac{1}{\sqrt{L}} \quad \psi_k^H \begin{pmatrix} 1 \\ e^{-s \Delta} \\ e^{-2s \Delta} \\ \vdots \\ e^{-s (M-1) \Delta} \end{pmatrix}$$
(11)

This orthogonal waveform-to-phasor map was discussed in detail in [8], where we set $\Delta = \frac{T}{2\,M}$ or, equivalently, $\xi = \frac{1}{2\,M}$. The following theorem establishes the fact that orthogonality of \mathcal{W}_M cannot be achieved when $0 < \xi < \frac{1}{2\,M}$.

Theorem 4.1 (Orthogonal \mathcal{W}_M): When the harmonic index set \mathcal{S} consists of odd harmonics, including the fundamental harmonic, the matrix \mathcal{W}_M is orthogonal for $\xi = \xi_{orth}(M) \stackrel{\triangle}{=} \frac{1}{2M}$, but is never orthogonal for $0 < \xi < \xi_{orth}(M)$.

Setting $\Delta = \frac{T}{2M}$ in (11) results in a very simple expression for $H_k(j\omega)$, with $H_k(jr\omega_0) = 0$ for most odd r values, as shown in the following Theorem.

Theorem 4.2 (Special $H_k(s)$): Consider the transfer function $H_k(s)$ defined by (11). A more compact expression for the frequency response $H_k(j\omega)$, for any $k \in \mathcal{S}$, is

$$H_k(j\omega) = \sqrt{2} \frac{\sin(\frac{\omega}{\omega_0} - k)\frac{\pi}{2}}{M\sin(\frac{\omega}{\omega_0} - k)\frac{\pi}{2M}} e^{-j(\frac{\omega}{\omega_0} - k)(\frac{M-1}{M})\frac{\pi}{2}}$$
(12)

Proof: see Appendix.

This expression for the frequency response is periodic, with period 2 M, and results in $|H_k(jr\omega_0)|=0$ for all odd values of r, except those that are periodic copies of k. We conclude that orthogonality results in suppression of many odd harmonics, significantly beyond those specified in Theorem 2.1.

Theorems 4.1 and 4.2 underscore the basic dichotomy in selecting the value of ξ : choosing $\xi = \frac{1}{2M} \equiv \xi_{orth}(M)$ makes \mathcal{W}_M orthogonal, inducing a Parseval property (see discussion in Section V), and it also results in reduced steady-state error. This is so because, for most odd r values $|H_k(jr\omega_0)|=0$, as discussed above, leading to a significant reduction in steady-state fluctuation of sub-cycle phasors. On the other hand, choosing a smaller value for ξ is desirable in applications where achieving a fast transient response is the primary objective, and a moderate steady-state error can be tolerated. The tradeoff between transient response and steady-state error is discussed in further detail in Section VI.

V. DYNAMIC POWER QUALITY METRICS (DPQMS)

We determine the sub-cycle (polyphase) voltage phasors $\{\widehat{V}_k(t);\ k\in\mathcal{S}\}$ from an acquired m-phase voltage waveform v(t), and similarly for the current waveform i(t). In order to facilitate compact presentation of our results, we now introduce the $1\times mL$ phasor arrays

$$\mathbf{V}(t) \stackrel{\triangle}{=} \left[\widehat{V}_{k_1}(t) \ \widehat{V}_{k_2}(t) \ \dots \ \widehat{V}_{k_L}(t) \right]$$

$$\mathbf{I}(t) \stackrel{\triangle}{=} \left[\widehat{I}_{k_1}(t) \ \widehat{I}_{k_2}(t) \ \dots \ \widehat{I}_{k_L}(t) \right]$$
(13)

where $\{\widehat{V}_{k_i}(t); 1 \leq i \leq L\}$ are the sub-cycle (polyphase) voltage phasors and $\{\widehat{I}_{k_i}(t); 1 \leq i \leq L\}$ are the sub-cycle current phasors (recall that $\mathcal{S} = \{k_1, k_2, \ldots, k_L\}$).

Motivated by the definitions of real power and rms voltage and current in terms of full-cycle phasors (see, e.g., [9]–[11]) we have introduced in [8] their sub-cycle counterparts, viz.,

$$P(t) \stackrel{\triangle}{=} \Re \left\{ \mathbf{V}(t) \ \mathbf{I}^{H}(t) \right\} = \sum_{k \in S} \Re \left\{ \widehat{V}_{k}(t) \ \widehat{I}_{k}^{H}(t) \right\}$$
(14a)

$$V_{rms}^{2}(t) \stackrel{\triangle}{=} \mathbf{V}(t) \mathbf{V}^{H}(t) = \sum_{k \in \mathcal{S}} \widehat{V}_{k}(t) \widehat{V}_{k}^{H}(t)$$
 (14b)

$$I_{rms}^{2}(t) \stackrel{\triangle}{=} \mathbf{I}(t) \, \mathbf{I}^{H}(t) = \sum_{k \in S} \widehat{I}_{k}(t) \, \widehat{I}_{k}^{H}(t)$$
 (14c)

and defined the sub-cycle apparent power

$$S(t) \stackrel{\triangle}{=} V_{rms}(t) I_{rms}(t)$$

A statistics-based approach was used in [8] to construct a 4-component decomposition of $S^2(t)$, viz.,

$$S^{2}(t) = P^{2}(t) + N_{q}^{2}(t) + Q^{2}(t) + N_{b}^{2}(t)$$
 (15)

A detailed derivation is provided in [8]. The key step is the introduction of the equivalent load admittance

$$\frac{\mathbf{I}(t)}{\mathbf{V}(t)} = \mathbf{G}(t) - j\mathbf{B}(t)$$

where the division of $\mathbf{I}(t)$ over $\mathbf{V}(t)$ is an element-by-element operation (equivalent to "./" division in MATLAB). The mean and variance of the $1 \times mL$ parameter sets $\mathbf{G}(t)$ and $\mathbf{B}(t)$ are then used to determine the four components in (15). In particular, the metric $N_g(t)$ (resp. $N_b(t)$) captures the variation of the elements of $\mathbf{G}(t)$ (resp. elements of $\mathbf{B}(t)$) across harmonics and phases. A similar approach was used in the full-cycle case to obtain a 7-component decomposition of apparent power [11].

In the special case $\xi = \frac{1}{2M} \equiv \xi_{orth}(M)$ the matrix \mathcal{W}_M is orthogonal (recall Theorem 4.1), which induces a *Parseval-type relation* between the time-domain waveform samples and the associated sub-cycle phasors: when $\mathcal{W}_M \mathcal{W}_M^H = I$, we obtain from (1) the identity

$$\frac{1}{2} tr \left\{ \begin{pmatrix} \widehat{V}_{k_1}(t) e^{jk_1\omega_0 t} \\ \vdots \\ \widehat{V}_{k_L}(t) e^{jk_L\omega_0 t} \\ \widehat{V}_{k_1}^*(t) e^{-jk_1\omega_0 t} \\ \vdots \\ \widehat{V}_{k_L}^*(t) e^{-jk_L\omega_0 t} \end{pmatrix} \begin{pmatrix} \widehat{I}_{k_1}(t) e^{jk_1\omega_0 t} \\ \vdots \\ \widehat{I}_{k_L}(t) e^{jk_L\omega_0 t} \\ \widehat{I}_{k_1}^*(t) e^{-jk_1\omega_0 t} \\ \vdots \\ \widehat{I}_{k_L}^*(t) e^{-jk_L\omega_0 t} \end{pmatrix} \right\}$$

$$= \frac{1}{M} tr \left\{ \begin{pmatrix} v(t) \\ v(t - \Delta_1) \\ \vdots \\ \vdots \\ v(t - \Delta_{M-1}) \end{pmatrix} \begin{pmatrix} i(t) \\ i(t - \Delta_1) \\ \vdots \\ \vdots \\ i(t - \Delta_{M-1}) \end{pmatrix}^{\top} \right\}$$
 (16)

where $tr\{$ } denotes the trace of a square matrix. The left-hand-side of this identity reduces to the expression $\sum_{k \in \mathcal{S}} \Re\{\widehat{V}_k(t) \ \widehat{I}_k^H(t) \}$ which, by definition, is the sub-cycle power P(t). The right-hand-side of the same identity yields the time-averaged expression $\frac{1}{M} \sum_{i=0}^{M-1} v(t-\Delta_i) i^\top (t-\Delta_i)$. Recalling that the product $p(t) = v(t) i^\top (t)$ is the instantaneous power, we conclude that, under the orthogonality constraint,

$$P(t) \stackrel{\triangle}{=} \sum_{k \in \mathcal{S}} \Re\{\widehat{V}_k(t) \widehat{I}_k^H(t)\} = \frac{1}{M} \sum_{i=0}^{M-1} p(t - \Delta_i) \quad (17)$$

In other words, the phasor-based sub-cycle power P(t) can also be determined by averaging the instantaneous power samples $\{p(t-\Delta_i); 0 \le i \le M-1\}$. Similar Parseval relations hold

for $V_{rms}(t)$ and $I_{rms}(t)$, viz.,

$$V_{rms}^{2}(t) \stackrel{\triangle}{=} \sum_{k \in \mathcal{S}} \widehat{V}_{k}(t) \ \widehat{V}_{k}^{H}(t) = \frac{1}{M} \sum v(t - \Delta_{i}) v^{\top}(t - \Delta_{i})$$

$$I_{rms}^{2}(t) \stackrel{\triangle}{=} \sum_{k \in \mathcal{S}} \widehat{I}_{k}(t) \ \widehat{I}_{k}^{H}(t) = \frac{1}{M} \sum_{k} i(t - \Delta_{i}) i^{\top}(t - \Delta_{i})$$

These results generalize to any value of M the Parseval relations that were established in [8] for the special case M=4.

The special choice $\xi = \frac{1}{2M}$ results in good performance in the presence of slow-transients (as well as in steady-state operation): see Example 1 in the following section. However, accurate estimation of the duration and moment of onset of fast wide-band transients requires a reduced value of ξ , as we demonstrate in Examples 2 and 3 in the following section.

VI. TRADEOFF BETWEEN ACCURACY AND AGILITY

We have observed in Section III that the presence of spurious harmonics causes steady-state fluctuations in all sub-cycle phasors, which tend to increase in strength as the value of ξ decreases away from $\xi_{orth}(M) \equiv \frac{1}{2\,M}.$ The sub-cycle real power $P_{sc}(t)$ exhibits similar behavior, since it inherits the steady-state fluctuations of the (sub-cycle) $\widehat{V}_k(t)$ and $\widehat{I}_k(t)$ phasors. We can use the dependence on ξ of the overall (rms) steady-state error

$$\Delta P_{ss} \stackrel{\triangle}{=} \sqrt{\left\langle \left(P_{sc}(t) - P_{fc,ss} \right)^2 \right\rangle}$$

to characterize the tradeoff between accuracy (=steady-state error) and agility (=transient response) of a chosen sub-cycle scheme, because both the group-delay and the bandwidth of the sub-cycle waveform-to-phasor map $H_k(s)$ are controlled by the value of ξ . Here we use the notation $P_{sc}(t)$ for the sub-cycle real power to distinguish it from its full-cycle counterpart, which we denote by $P_{fc}(t)$. Also, $P_{fc,ss} = \sum_{k=1}^{\infty} V_k I_k^H$ is the standard (full-cycle) real power in steady-state operation, and $\langle \cdot \rangle$ denotes averaging over a single cycle.

Our ongoing empirical studies demonstrate that increasing ξ above $\frac{1}{2\,M}$ always results in performance degradation. Thus we consider in the sequel only the range $0<\xi\leq\frac{1}{2\,M}$. The optimal value of $\Delta P_{ss}/P_{fc,ss}$, obtained using M=4 and the best \mathcal{S} -choice for each value of ξ , is shown in Fig. 2 for a synthetic example involving a balanced 3-phase RL load, fed by a balanced voltage containing the 1-st, 5-th, 7-th and 13-th harmonics. We observe that ΔP_{ss} tends to increase as the value of ξ is reduced from $\xi_{orth}(M)\equiv\frac{1}{2\,M}$ towards zero. However, the change in ΔP_{ss} is relatively small over the range $0.06<\xi<0.125\equiv\xi_{orth}(4)$: this observation suggests that ξ can be reduced by a factor of 2 (at least) without incurring a significant increase in ΔP_{ss} . This is desirable in applications where the primary concern is a fast transient response, which can be achieved by reducing the value of ξ .

We illustrate the versatility of our sub-cycle power quality metrics via one synthetic and two real-life examples: (i) an extended (15-cycle) slowly-evolving sub-station transient, (ii)

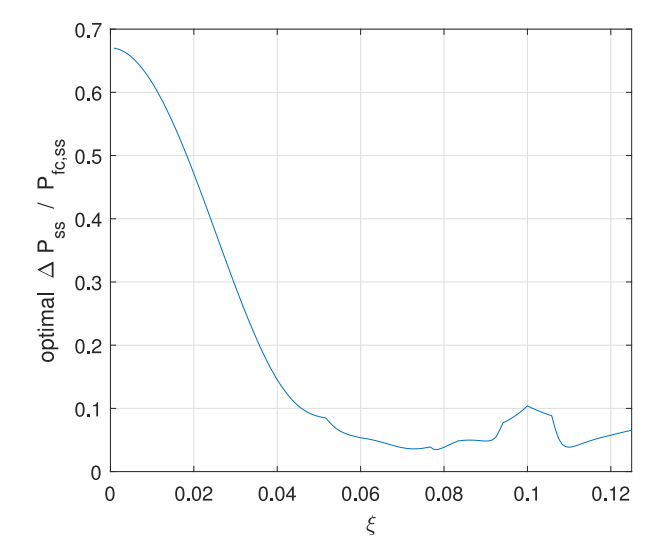


Fig. 2. Optimal $\Delta P_{ss}/P_{fc,ss}$ as a function of ξ .

a short (single-cycle) wide-band capacitor switching transient, and (iii) a synthetic injected short transient.

Example 1 (Sub-station transient): This real-world transient was obtained from the collection of data sets recorded at the 20MVA Butantã distribution sub-station belonging to the AES Eletropaulo utility in Brazil. The sampling frequency of the recorded transient waveforms is 960 Hz, i.e., 16 samples/cycle. To facilitate calculation of DPQMs, we resampled voltage and current waveforms digitally, at 256 samples/cycle.

This extended transient event involves a relatively short voltage sag in phase "a," and moderate/long voltage sags in phases "b" and "c". These result in current surges of similar lengths, apparently leading to a shutdown of the sub-station. The resulting waveforms are shown in Fig. 3. We notice that the sub-cycle $P_{sc}(t)$ waveforms for $\xi = \xi_{orth}(M)$ match their full-cycle counterpart in the steady-state interval that precedes the transient. Both waveforms behave similarly also within the transient interval, and the same observation holds for the other three DPQMs. Thus the main advantage of the sub-cycle scheme in this case is the significant reduction in computational cost, as compared with the full-cycle approach: see [8] for a detailed cost comparison between the sub-cycle and the full-cycle schemes. However, in general, sub-cycle metrics provide more accurate information about the transient, as we demonstrate in the following two examples.

Example 2 (Wind farm oscillatory transient [12]): This real-world transient case was provided by the National Renewable Energy Laboratory (NREL), and collected from the Trent Mesa Wind Farm in Texas. A short (≈one cycle) oscillatory transient is caused by switching in a bank of shunt capacitors. The sampling frequency of the recorded transient waveforms is 7.676 kHz, i.e., 127.9 samples/cycle [12]. As explained in Example 1, we resampled all waveforms at the rate of 256 samples/cycle.

The resulting dynamic power waveforms are shown in Fig. 4. The sub-cycle dynamic power $P_{sc}(t)$ matches its full-cycle counterpart $P_{fc}(t)$ in the steady-state interval preceding the onset of the transient (i.e., $t \le 0.031$ sec). However, these two

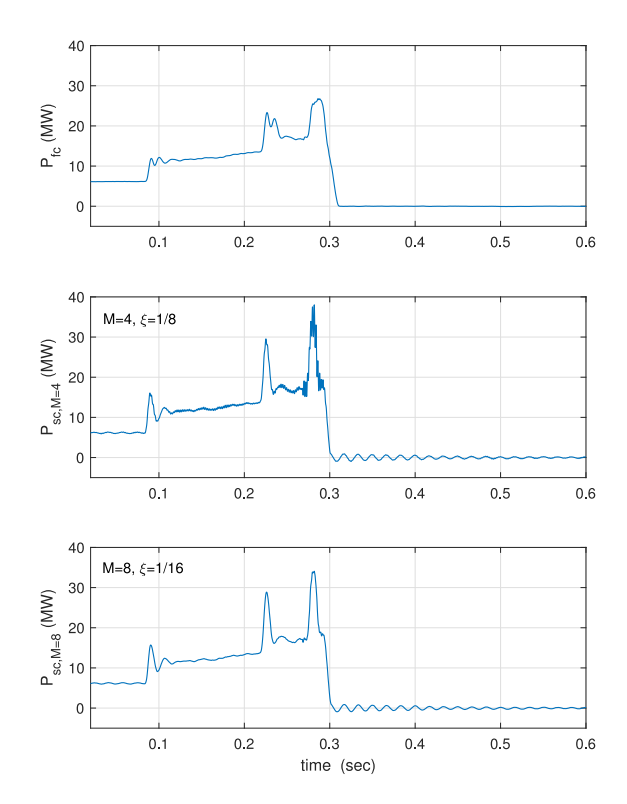


Fig. 3. Example 1: P-metric waveforms.

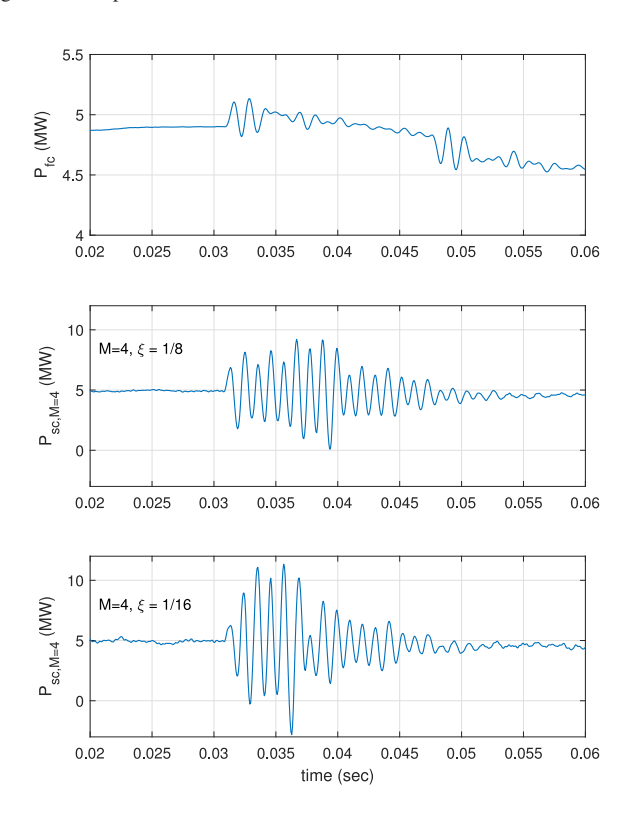


Fig. 4. Example 2: P-metric waveforms.

power metrics differ greatly within the transient interval (i.e., in $0.031~{\rm sec} \le t \le 0.048~{\rm sec}$): the sub-cycle $P_{sc}(t)$ exhibits a sizeable transient component, comparable to its steady-state component, while the transient component of the full-cycle

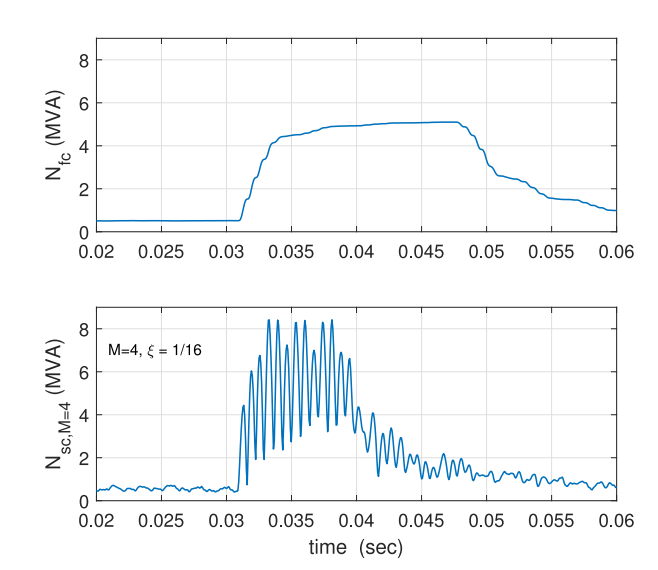


Fig. 5. Example 2: N-metric waveforms.

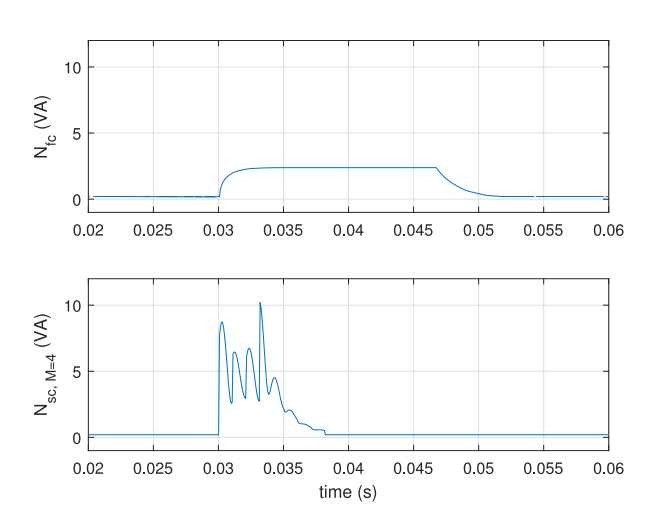


Fig. 6. Example 3: N-metric waveforms.

 $P_{fc}(t)$ is barely perceptible (notice the difference in the vertical scale used in the top plot of Fig. 4).

Since none of the metrics in Fig. 4 provides accurate information about the duration of the transient, we propose to use instead the *combined N-metric* $N(t) \stackrel{\triangle}{=} \sqrt{N_g^2(t) + N_b^2(t)}$, which can be viewed as the sub-cycle equivalent of Budeanu's "distortion power." We note that the full-cycle $N_{fc}(t)$ tends to exaggerate the duration of the transient interval (Fig. 5). In contrast, the sub-cycle $N_{sc}(t)$, obtained with $\mathcal{S} = \{1,5\}$ and $\xi = \frac{1}{16} \equiv \frac{1}{2} \xi_{orth}(4)$, identifies two distinct transient sub-intervals: (i) a strong transient in $0.031 \sec \le t \le 0.040 \sec$, and (ii) a decaying weaker transient in $0.040 \sec \le t \le 0.048 \sec$. The same two sub-intervals can also be discerned from the bottom plot in Fig. 4.

Example 3 (Synthetic short transient [13]): This synthetic data-set was generated by injecting a decaying 15-th harmonic component, limited to the short time-interval $0.03 \sec \le t \le 0.035 \sec$, into a steady-state waveform consisting of an unbalanced fundamental, and a much smaller 5-th harmonic (about

10% of the fundamental). The sampling frequency of the generated waveforms is 15.36 kHz, i.e., 256 samples/cycle.

Again we note that in this synthetic example the full-cycle $N_{fc}(t)$ greatly exaggerates the duration of the transient interval (Fig. 6). In contrast, the sub-cycle $N_{sc}(t)$, obtained with $\mathcal{S} = \{1,5\}$ and $\xi = \frac{1}{16} \equiv \frac{1}{2} \, \xi_{orth}(4)$, identifies correctly both the duration and the time of onset of the injected transient. Notice also that the response to the onset of a fast (wide-band) transient is almost instantaneous: although the group-delay in this example is about 0.003 sec, the response in Fig. 6, for both full-cycle and sub-cycle, shows no such delay. This property of the sub-cycle N-metric could be very desirable in protection applications.

VII. CONCLUDING REMARKS

We have extended the sub-cycle approach of [8] to allow an arbitrary shift Δ between the waveform samples used to construct sub-cycle dynamic phasors. The scheme presented in [8] relied on the special choice $\xi = \frac{1}{2M}$ of the normalized shift, which ensures low steady-state error, and induces a Parseval relation between waveform samples and sub-cycle dynamic phasors. We have shown, however, that the transient response of sub-cycle dynamic power metrics can be improved by reducing the value of ξ towards $\frac{1}{4M}$, and using fewer waveform samples. Our real-life examples demonstrate that adjustment of the normalized shift ξ can be very effective in the presence of short wide-band transients: the N-metric obtained from a 4-sample sub-cycle scheme with $\xi = \frac{1}{16}$ provides very accurate information about the duration and onset-time of a transient. We have also derived a range of ξ -values for which the steady-state error remains near-optimal, and demonstrated that excellent performance for slow transients (and in steady-state) is achieved when M=8and $\xi = \frac{1}{2M}$.

Taken together, our results suggest that in practical real-time implementations it may be advantageous to calculate at least two sets of phasors to adequately cover slow and fast transients. Given the low cost of each sub-cycle calculation, the overall computational effort of such a scheme is still significantly below that of full-cycle calculations, while providing improved metrics for various classes of transients. The approach presented here also has advantages vis-a-vis Akagi-type instantaneous power metrics and their derivatives in terms of a comparable cost, but much lower steady-state fluctuation; we plan to explore and quantify this aspect in our future work.

APPENDIX

Proof of Theorem 2.1: Starting with the definition (3b), we evaluate the frequency response $H_{k_i}(j\omega)$ at the (harmonic) frequency $\omega = \ell \omega_0$, for any harmonic index $\ell \in \mathcal{S}$, viz.,

$$H_{k_i}(j\ell\omega_0) = \frac{1}{\sqrt{L}} e_i \mathcal{W}_M^{-1} \begin{pmatrix} 1\\ e^{-j\ell\omega_0 \Delta_1} \\ e^{-j\ell\omega_0 \Delta_2} \\ \vdots \\ e^{-j\ell\omega_0 \Delta_{M-1}} \end{pmatrix}, \ 1 \le i \le L$$

where $e_i \stackrel{\triangle}{=} [\underbrace{0 \dots 0}_i \underbrace{1}_i 0 \dots 0]$. We observe (from (2)) that

$$\begin{pmatrix} 1 \\ e^{-j\ell\omega_0 \, \Delta_1} \\ e^{-j\ell\omega_0 \, \Delta_2} \\ \vdots \\ e^{-j\ell\omega_0 \, \Delta_{M-1}} \end{pmatrix} = \sqrt{M} \, \psi_{\ell} = \sqrt{M} \, \mathcal{W}_M \, e_j^{\top}$$
 (18)

where $\ell = k_j$ (i.e., ℓ is the j-th harmonic index in S), and thus

$$H_{k_i}(jk_j\omega_0) = \frac{\sqrt{M}}{\sqrt{L}} \ e_i \ \mathcal{W}_M^{-1} \ \mathcal{W}_M \ e_j^{\top} = \sqrt{2} \ e_i \ e_j^{\top} = \sqrt{2} \ \delta_{ij}$$

Therefore, for every $k \in \mathcal{S}$ and every $\ell \in \mathcal{S}$, we have the property (4a). Similarly, $H_{k_i}(-jk_j\,\omega_0)$ involves $\psi_{k_j}^* = \mathcal{W}_M\,e_{j+L}^\top$ so that $H_{k_i}(-jk_j\,\omega_0) = \sqrt{2}\,e_i\,e_{j+L}^\top = 0$, which establishes the property (4b).

Proof of Theorem 3.1: Setting $\Delta_i = i\Delta$ and $e^{s\Delta} = \zeta$ in (3b) allows us to interpret $H_k(s)$ as a polynomial of degree M-1 in ζ^{-1} , viz.,

$$\mathcal{H}_{k_i}(\zeta) \stackrel{\triangle}{=} \frac{1}{\sqrt{L}} e_i \, \mathcal{W}_M^{-1} \begin{pmatrix} 1 \\ \zeta^{-1} \\ \zeta^{-2} \\ \vdots \\ \zeta^{-(M-1)} \end{pmatrix}$$

so that

$$H_k(s) = \mathcal{H}_k(\zeta) \bigg|_{\zeta = e^{s\Delta}}$$
 (19)

Now, since $H_k(j\ell\omega_0)=0$ for certain values of ℓ (recall (4)), it follows that (for every $k\in\mathcal{S}$)

$$\mathcal{H}_k(\zeta)\bigg|_{\zeta=e^{j\ell\omega_0\Delta}}=0\tag{20a}$$

for the same values of ℓ . Notice that (20a) holds for $2L-1\equiv M-1$ values of ℓ , because

- eq. (4a) holds for the L-1 distinct values defined by $\ell \in \mathcal{S}, \ell \neq k$
- eq. (4b) holds for the L distinct values defined by $\ell \in \mathcal{S}$. Thus the expression (20a) enumerates all M-1 zeros (= roots) of the polynomial $\mathcal{H}_k(\zeta)$. In addition, we have the constraint

$$\mathcal{H}_k(\zeta)\Big|_{\zeta=e^{jk\omega_0\Delta}} = H_k(jk\omega_0) = \sqrt{2}$$
 (20b)

Since deg $\mathcal{H}_k(\zeta) = M - 1$, the constraints (20) provide all the information needed to obtain an explicit (matrix-free) expression for the polynomial $\mathcal{H}_k(\zeta)$, viz.,

$$\mathcal{H}_k(\zeta) = \mathcal{C}_k \left(1 - e^{-jk\omega_0 \Delta} \zeta^{-1} \right)$$

$$\times \prod_{\ell \in \mathcal{S}, \ \ell \neq k} \left(1 - e^{j\ell\omega_0 \Delta} \zeta^{-1} \right) \left(1 - e^{-j\ell\omega_0 \Delta} \zeta^{-1} \right)$$

where the value of the scaling coefficient C_k can be determined from (20b). This establishes the result (8a). In view of (19), it now follows that (for every $k \in S$)

$$H_k(j\omega) = \mathcal{C}_k \left(1 - e^{-jk\omega_0 \Delta} e^{-j\omega \Delta} \right)$$

$$\times \prod_{\ell \in \mathcal{S}, \ \ell \neq k} \left(1 - e^{-j(\omega + \ell\omega_0) \Delta} \right) \left(1 - e^{-j(\omega - \ell\omega_0) \Delta} \right)$$

We can also express the frequency response $H_k(j\omega)$ in terms of the normalized shift $\xi = \frac{\Delta}{T}$ (so that $\omega_0 \Delta = 2\pi \xi$) and the normalized frequency $(\frac{\omega}{\omega_0})$, viz.,

$$H_k(j\omega) = \widehat{\mathcal{C}}_k \ e^{-j(\frac{\omega}{\omega_0} - k)(M - 1)\pi\xi} \ \sin\left(\frac{\omega}{\omega_0} + k\right) \pi\xi$$
$$\times \prod_{\ell \in \mathcal{S}} \min\left(\frac{\omega}{\omega_0} + \ell\right) \pi\xi \cdot \sin\left(\frac{\omega}{\omega_0} - \ell\right) \pi\xi$$

with the value of the scaling coefficient \widehat{C}_k determined from (20b), namely

$$\widehat{\mathcal{C}}_k = \frac{\sqrt{2}}{\sin(2\pi k \, \xi) \, \prod_{\ell \in \mathcal{S}, \, \ell \neq k} \, \sin(k + \ell) \pi \xi \cdot \sin(k - \ell) \pi \xi}$$

This establishes the result (8b).

Proof of Theorem 4.1: The matrix \mathcal{W}_M is orthogonal if (and only if) every pair of its columns is orthogonal, namely $\psi_\ell^H \psi_k = \delta_{k,\ell}$ and $\left[\psi_\ell^*\right]^H \psi_k = 0$ for every $k \in \mathcal{S}$ and every $\ell \in \mathcal{S}$. It follows from (7) that

$$\psi_{\ell}^{H} \psi_{k} = \frac{1}{M} \sum_{i=0}^{M-1} (\alpha_{\ell}^{*} \alpha_{k})^{i} = \frac{1}{M} \frac{1 - e^{-j(k-\ell)2\pi M\xi}}{1 - e^{-j(k-\ell)2\pi\xi}}$$

which vanishes for $\xi=\frac{1}{2\,M}$ (when $k\neq \ell$) because $k-\ell$ is even, and so $e^{-j(k-\ell)2\pi M\xi}|_{\,\xi=1/(2\,M)}=e^{-j(k-\ell)\pi}=1$, while $e^{-j(k-\ell)2\pi\xi}|_{\,\xi=1/(2\,M)}=e^{-j(k-\ell)\pi/M}\neq 1$. Similarly,

$$\left[\psi_{\ell}^{*}\right]^{H} \psi_{k} = \frac{1}{M} \sum_{i=0}^{M-1} (\alpha_{\ell} \, \alpha_{k})^{i} = \frac{1}{M} \, \frac{1 - e^{-j(k+\ell)2\pi M \xi}}{1 - e^{-j(k+\ell)2\pi \xi}}$$

which vanishes (for the same reasons) when $\xi = \frac{1}{2M}$, because $k + \ell$ is also even. Thus, \mathcal{W}_M is always orthogonal when $\xi = \frac{1}{2M}$.

However, when $0 < \xi < \frac{1}{2M}$, some of the conditions $\psi_\ell^H \psi_k = \delta_{k,\ell}$ and $\left[\psi_\ell^*\right]^H \psi_k = 0$ are violated. In particular, we observe that

$$\left[\psi_1^*\right]^H \psi_1 = \frac{1}{M} \sum_{i=0}^{M-1} (\alpha_1 \, \alpha_1)^i = \frac{1}{M} \, \frac{1 - e^{-j4\pi M\xi}}{1 - e^{-j4\pi\xi}} \neq 0$$

because $0 < 4\pi M \xi < 2\pi$, and thus $e^{-j4\pi M \xi} \neq 1$, leading to the conclusion that the matrix \mathcal{W}_M can never be orthogonal for $\xi < \frac{1}{2M}$.

Proof of Theorem 4.2: Using the expression (7) for ψ_k and the fact that now $\alpha_k^*=e^{j\frac{k\pi}{M}}$, the transfer function $H_k(s)$ of (11)

can be written as

$$H_k(s) = \frac{1}{\sqrt{L}} \cdot \frac{1}{\sqrt{M}} \sum_{i=0}^{M-1} \left(e^{j\frac{k\pi}{M}} \right)^i e^{-i\frac{sT}{2M}}$$
$$= \frac{\sqrt{2}}{M} \cdot \frac{1 - \left(e^{j\frac{k\pi}{M}} e^{-\frac{sT}{2M}} \right)^M}{1 - e^{j\frac{k\pi}{M}} e^{-\frac{sT}{2M}}}$$

Setting $s=j\omega$, and using the relation $T=\frac{2\pi}{\omega_0}$, we obtain the expression (12) for the frequency response $H_k(j\omega)$, viz.,

$$H_k(j\omega) = \frac{\sqrt{2}}{M} \cdot \frac{1 - e^{jk\pi} e^{-j\frac{\omega}{\omega_0}\pi}}{1 - e^{j\frac{k\pi}{M}} e^{-j\frac{\omega}{\omega_0}\pi}}$$
$$= \frac{\sqrt{2}}{M} \cdot \frac{e^{-j(\frac{\omega}{\omega_0} - k)\frac{\pi}{2}}}{e^{-j(\frac{\omega}{\omega_0} - k)\frac{\pi}{2M}}} \cdot \frac{\sin(\frac{\omega}{\omega_0} - k)\frac{\pi}{2}}{\sin(\frac{\omega}{\omega_0} - k)\frac{\pi}{2M}}$$

REFERENCES

- [1] P. Top and J. Breneman, "Compressing phasor measurement data," in *Proc. North Amer. Power Symp.*, Manhattan, KS, USA, 2013, pp. 1–4.
- [2] L. Chu, R. Qiu, X. He, Z. Ling, and Y. Liu, "Massive streaming PMU data modeling and analytics in smart grid state evaluation based on multiple high-dimensional covariance test," *IEEE Trans. Big Data*, vol. 4, no. 1, pp. 55–64, Jan. 2018.
- [3] M. K. Penshanwar, M. Gavande, and M. F. A. R. Satarkar, "Phasor measurement unit technology and its applications—A review," in *Proc. Int. Conf. Energy Syst. Appl.*, Nov. 2015.
- [4] F. Zhang, L. Cheng, X. Li, Y. Sun, W. Gao, and W. Zhao, "Application of a real-time data compression and adapted protocol technique for WAMS," *IEEE Trans. Power Syst.*, vol. 30, no. 2, pp. 55–64, Mar. 2015.
- [5] M. M. N. Aravind, L. S. Anju, and R. Sunitha, "Application of compressed sampling to overcome big data issues in synchrophasors," in *Proc. 6th IEEE Int. Conf. Power Syst.*, New Delhi, India, 2016, pp. 1–5.
- [6] T. Xu and T. Overbye, "Real-time event detection and feature extraction using PMU measurement data," in *Proc. IEEE Int. Conf. Smart Grid Commun.*, Miami, FL, USA, 2015, pp. 265–270.
- [7] A. C. Gilbert, P. Indyk, M. Iwen, and L. Schmidt, "Recent developments in the sparse fourier transform," *IEEE Signal Process. Mag.*, vol. 31, no. 5, pp. 91–100, Sep. 2014.
- [8] A. Ghanavati, H. Lev-Ari, and A. M. Stanković, "A sub-cycle approach to dynamic phasors with application to dynamic power quality metrics," *IEEE Trans. Power Del.*, vol. 33, no. 5, pp. 2217–2225, Oct. 2018.
- [9] H. Lev-Ari and A. M. Stanković, "A decomposition of apparent power in polyphase unbalanced networks in non-sinusoidal operation," *IEEE Trans. Power Syst.*, vol. 21, no. 1, pp. 438–440, Feb. 2006.
- [10] H. Lev-Ari, A. M. Stanković, and S. J. Ceballos, "An orthogonal decomposition of apparent power with application to an industrial load," in *Proc. Power Syst. Comput. Conf.*, Liege, Belgium, Aug. 2005.
- [11] H. Lev-Ari, A. M. Stanković, and A. Ghanavati, "Dynamic decomposition of apparent power in polyphase unbalanced networks with application to transients in an industrial load," in *Proc. 40th North Amer. Power Symp.*, Calgary, AB, Canada, Sep. 2008.
- [12] M. Islam, H. A. Mohammadpour, A. Ghaderi, C. W. Brice, and Y.-J. Shin, "Time-frequency-based instantaneous power components for transient disturbances according to IEEE Standard 1459," *IEEE Trans. Power Del.*, vol. 30, no. 3, pp. 1288–297, Jun. 2015.
- [13] A. Ghanavati, "A sub-cycle approach to dynamic phasors with application to dynamic power quality metrics," Ph.D. dissertation, Dept. Elect. Comput. Eng., Northeastern Univ., Boston, MA, USA, May 2018.



Afsaneh Ghanavati (S'16–M'18) received the B.S. degree in electrical engineering from Shiraz University, Shiraz, Iran, in 1998, and the M.S. and the Ph.D. degrees in electrical engineering from Northeastern University, Boston, MA, USA, in 2012 and 2018 respectively. She is currently an Assistant Professor with the Department of Electrical and Computer Engineering, Wentworth Institute of Technology, Boston, MA, USA. Her present areas of interest include power systems, signal processing, dynamic phasors and power quality. She has been a member of

the Eta Kappa Nu, Engineering Honor Society and is a member of IEEE Power & Energy Society.



Hanoch Lev-Ari (M'84–SM'93–F'05) received the B.S. degree (Summa Cum Laude), and the M.S. degree both in electrical engineering from the Technion, Israel Institute of Technology, Haifa, Israel, in 1971 and 1978, respectively, and the Ph.D. degree in electrical engineering from Stanford University, Stanford, CA, USA, in 1984. He is currently a Professor with the Department of Electrical and Computer Engineering, Northeastern University, Boston, MA, USA. During 1994–1996, he was also the Director of the Communications and Digital Signal Process-

ing Center, Northeastern University. Before joining Northeastern, he was an Adjunct Research Professor of electrical engineering with Naval Postgraduate School, Monterey, CA, USA and a Senior Research Associate with Information Systems Laboratory at Stanford University. His present interests include adaptive filtering under the non-stationary regime, dynamic time-frequency analysis, and multi-rate/multi-sensor networked state estimation, with applications to identification of time-variant systems, customized dynamic phasors, dynamic power decomposition, and adaptive power flow control in polyphase power systems. He was an Associate Editor for the *Circuits, Systems and Signal Processing*, and of the IEEE TRANSACTIONS ON CIRCUITS AND SYSTEMS I, and is a member of SIAM.



Aleksandar M. Stanković (F'05) received the the Ph.D. degree in electrical engineering from the Massachusetts Institute of Technology, Cambridge, MA, USA, in 1993. He is currently as A.H. Howell Professor with Tufts University, Medford, MA, USA. He was with Northeastern University, Boston 1993—2010. He serves as an Associate Editor for the IEEE TRANSACTIONS ON POWER SYSTEMS. He has previously served the IEEE TRANSACTIONS ON SMART GRID, ON POWER SYSTEMS AND ON CONTROL SYSTEM TECHNOLOGY in the same capacity. He has held

visiting positions at United Technologies Research Center (sabbaticals in 2000 and 2007) and at L'Universite de Paris-Sud and Supelec (in 2004). He is a Co-Editor of book series on *Power Electronics and Power Systems for Springer*.